5.2 Thermohaline ocean circulation

Water, that is dense enough to sink from the surface to the bottom, is formed when cold air blows across the ocean at high latitudes in winter in the northern North Atlantic (e.g. in the Labrador Sea and between Norway and Greenland) and near Antarctica. The wind cools and evaporates water. If the wind is cold enough, sea ice forms, further increasing the salinity of the water because sea ice is fresher than sea water and salty water remains in the water when ice is formed. Bottom water is produced only in these regions, and the deep ocean is affected by these deep water formation processes. In other regions, cold, dense water is formed, but it is not quite salty enough to sink to the bottom. At mid and low latitudes, the density, even in winter, is sufficiently low that the water cannot sink more than a few hundred meters into the ocean. The only exception are some seas, such as the Mediterranean Sea, where evaporation is so great that the salinity of the water is sufficiently great for the water to sink to intermediate depths in the seas. If these seas are can exchange water with the open ocean, the waters formed in winter in the seas spreads out to intermediate depths in the ocean. Detailed measurements of the Atlantic current structure were made by an expedition of the research vessel Meteor from 1925-1927. On the basis of these data, Wüst [1935] characterized water masses necessary to describe the Atlantic currents and tracer distribution (Fig. 5.13). Broecker proposed a circulation model based on findings of the Meteor and other expeditions. In his model, large-scale oceanic circulation is represented by the transport system of a conveyor belt (Fig. 5.11) [Broecker and Peng, 1982].

The oceans carry about one third to one half the heat out of the tropics needed to maintain earth's temperature. Heat carried by the Gulf Stream and the North Atlantic drift warms the North Atlantic, keeping it ice free in winter, and it helps warm Europe. Norway, at 60°N is far warmer than southern Greenland or northern Labrador at the same latitude. Palm trees grow on the west coast of Ireland, but not in Newfoundland which is further south. The oceanic component of the heat-transport system is also called the Global Conveyor Belt. The basic idea is that the Gulf Stream carries heat to the North Atlantic realm. There the surface water releases heat and water to the atmosphere. Some of the ocean water becomes sufficiently cold, salty, and dense that it sinks

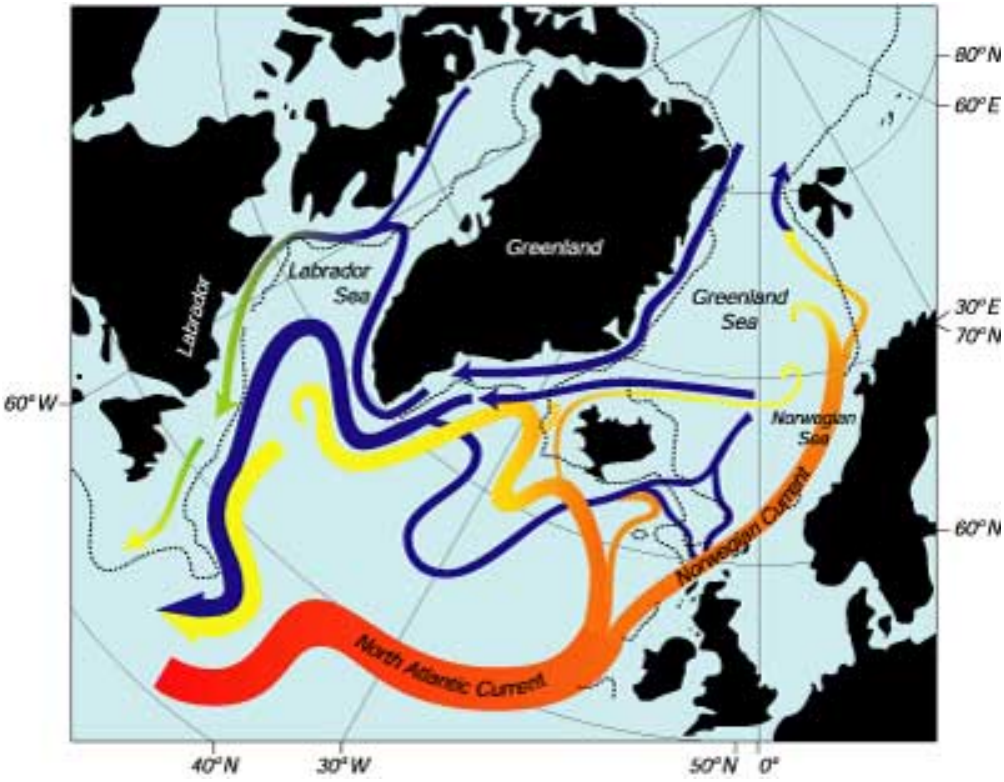

Figure 5.10: The surface (red, orange, yellow) and deep (violet, blue, green) currents in the North Atlantic. The North Atlantic Current brings warm water northward where it cools. Some sinks and returns southward as a cold, deep, western-boundary current. Some returns southward at the surface. From Woods Hole Oceanographic Institution.

to the bottom in the Norwegian and Greenland Seas. It then flows southward in very cold, bottom currents along western boundaries as a western boundary current. Some of the water remains at the surface and returns to the south in cool surface currents such as the Labrador Current and the Portugal Current (see Fig. 5.10).

The deep bottom water from the North Atlantic is mixed upward in other regions and ocean, and eventually it makes its way back to the Gulf Stream and the North Atlantic. Thus most of the water that sinks in the North Atlantic must be replaced by water from the far South Atlantic. As this surface water moves northward across the equator and eventually into the Gulf Stream, it carries heat out of the south Atlantic. So much heat is pulled northward by the formation of north-Atlantic bottom water in winter that heat transport in the Atlantic is entirely northward, even in the

southern hemisphere. Much of the solar heat absorbed by the tropical Atlantic is shipped north to warm Europe and the Northern Hemisphere. Imagine then what might happen if the supply of heat is shut off. We will get back to that topic in the next section, applying the box model.

We can make a crude estimate of the importance of the conveyor-belt circulation from a simple calculation. The Gulf Stream carries 40 Sv of $\mathbf{18}$°C water northward. Of this, 15 Sv return southward in the deep western boundary current at a temperature of 2°C. The flow carried by the conveyor belt must therefore lose 1 Petawatts (1 Petawatt = $\mathbf{10^{15}}$ Watt = 1 PW) in the North Atlantic north of 24°N. Although the calculation is very crude, it is remarkably close to the value of $\mathbf{1.2 \pm 0.2}$ PW estimated by Rintoul and Wunsch (1991). Calculation: Exercise 46.

The production of bottom water is influenced by the salinity of surface waters in the North Atlantic. It is also influenced by the rate of upwelling due to mixing in other oceanic areas. First, let's look at the influence of salinity. Saltier surface waters form denser water in winter than less salty water. At first you may think that temperature is also important, but at high latitudes water in all ocean basins gets cold enough to freeze, so all ocean produce -2°C water at the surface. Of this, only the most salty will sink, and the saltiest water is in the Atlantic and under the ice on the continental shelves around Antarctica.

The the conveyor is driven by deepwater formation in the northern North Atlantic, making it the engine of conveyor belt circulation. The conveyor belt metaphor necessarily simplifies the ocean system, it is of course not a full description of the deep ocean circulation, it contains different aspects of it [Brüning and Lohmann, 1999]. Broecker's [Broecker, 1987; Broecker et al., 1991] concept provides a successful approach for global ocean circulation, although several features can be wrong like the missing Antarctic bottom water, the upwelling areas etc.. However, the global conveyor belt metaphor inspired new ideas of halting or reversing the ocean circulation and put it into a global climate context [Bryan, 1986]. This was helpful for the interpretation of Greenland ice core records (Fig. **??**) indicating different climate states with different ocean modes of operation (like on and off states of a mechanical maschine). From the analogy, it was possible to a) identify the relevance of North Atlantic deep water production and b) realize the possibility of multiple

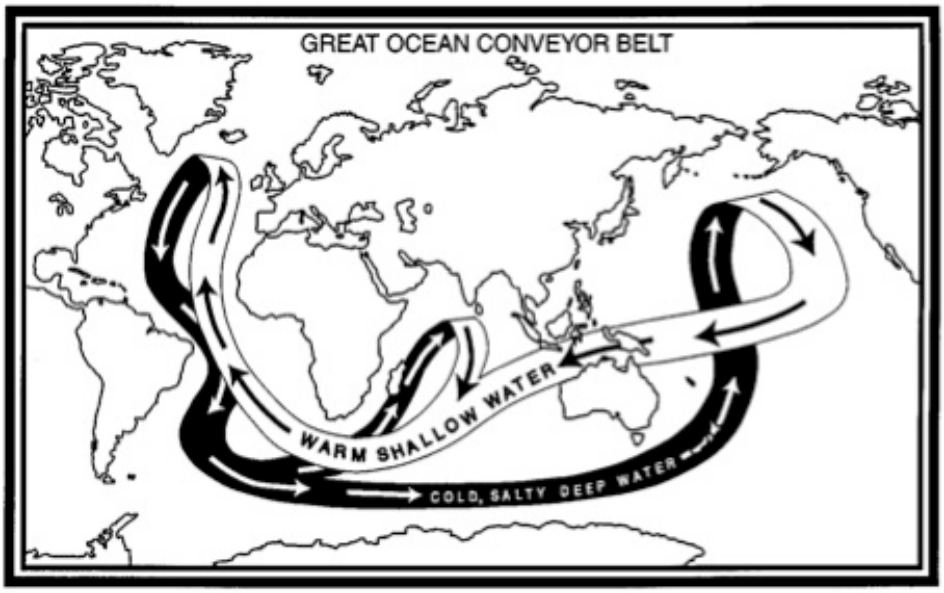

Figure 5.11: The great ocean conveyor [Broecker et al., 1991]. Warm and salty water entering the North Atlantic region is cooled. The dense water formed at the surface is convected to the deep ocean and is part of the southward return flow.

equilibria of ocean circulation states and their association with two different climatic states.

Many terms have been used to describe the deep circulation[5] and is called meridional overturning circulation. It is the zonal integral of the flow of mass plotted as a function of depth and latitude:

$$\tilde{v} = -\frac{\partial \psi}{\partial z} \tag{5.76}$$

$$\tilde{w} = \frac{\partial \psi}{\partial y} \tag{5.77}$$

with the zonally integrated velocities $\tilde{v}, \tilde{w}$, and a streamfunction $\psi(y, z)$ for the overturning circulation.

Figure 5.12 shows the meridional overturning circulation streamfunction $\psi(y, z)$ in the At-

[5] Abyssal circulation; Thermohaline circulation; Meridional overturning circulation; and Global conveyor. The term thermohaline circulation was once widely used, but it has disappeared almost entirely from the oceanographic literature. It is no longer used because it is clear that the flow is not only density driven.

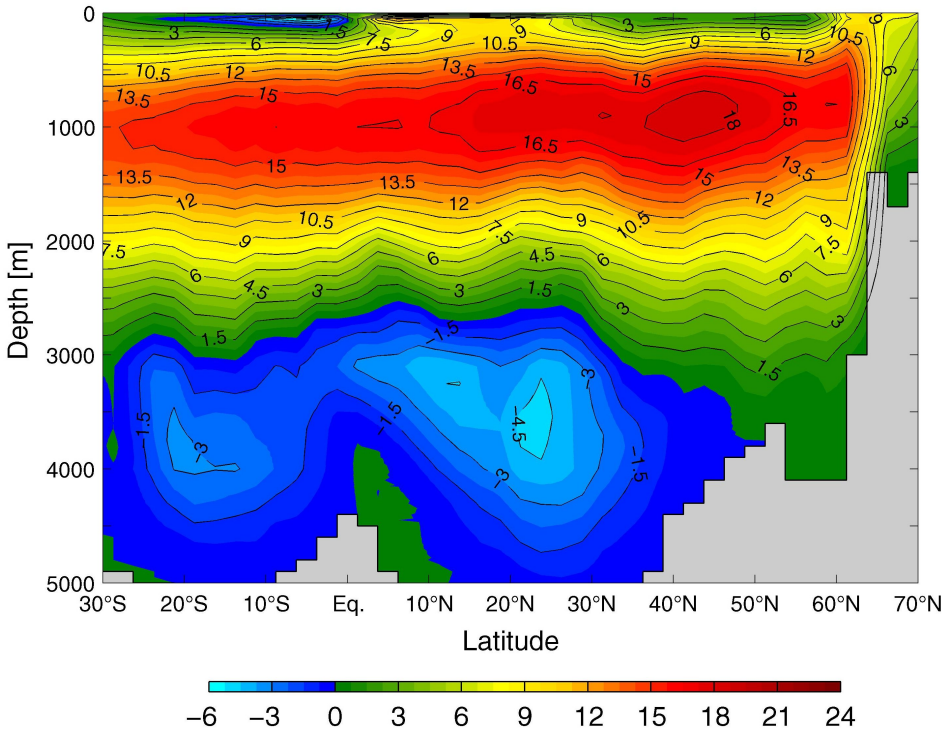

Figure 5.12: Modelled meridional overturning streamfunction in Sv ($1\ \mathrm{Sv} \equiv \mathbf{10^6}\ \mathrm{m^3 s^{-1}}$) in the Atlantic Ocean. Grey areas represent zonally integrated smoothed bathymetry.

lantic. The streamfunction is calculated as a cumulative sum of zonally integrated mass transports of the ocean at each latitude from surface to the particular depth. The zonally intregrated mass transport at a certain latitude derives from the zonally averaged meridional velocity component times the height of the ocean layer and the width of the ocean. Water flows along the stream lines. For instance, increasing positive values of MOC from surface to about 1,000m depth at mid latitudes of the Northern Hemisphere denote northward flowing water. With increasing depth the values of the MOC streamfunction decrease until a minimum at about 4,000m depth is reached. These waters move southward instead. In the Atlantic two major, a shallower and a deeper overturning cell exist according to figure 5.12. One cell shows positive values, thus, clockwise volume transport and stretches from almost the surface to about 2,500 - 3,000m depth. The other expands from about 3,000m depth to the bottom of the ocean at latitudes south of 40°N. The shallower cell denotes the modelled equivalent of North Atlantic Deep Water (NADW) while Antarctic Bottom

Water (AABW), transporting Southern Ocean water into the Atlantic, is simulated by the deeper cell. An overturning maximum of 18.7 Sv (1 Sv $\equiv \mathbf{10^6}$ $\mathrm{m^3 s^{-1}}$) is found at 40°- 50°N and 1,000m depth and an export into the Southern Ocean across 30°S of 14.9 Sv. This results in an overturning ratio of 0.79, so only little recirculation occurs. A closer look at Figure 5.12 reveals that NADW is predominantly formed north of 60°N with about 10 Sv. The inflow of AABW into the Atlantic is much weaker than the outflow of NADW. At 30°S a value of less than 1 Sv is calculated by the model while the maximum counter-clockwise overturning of the bottom water cell reaches 4.7 Sv at 25°N.

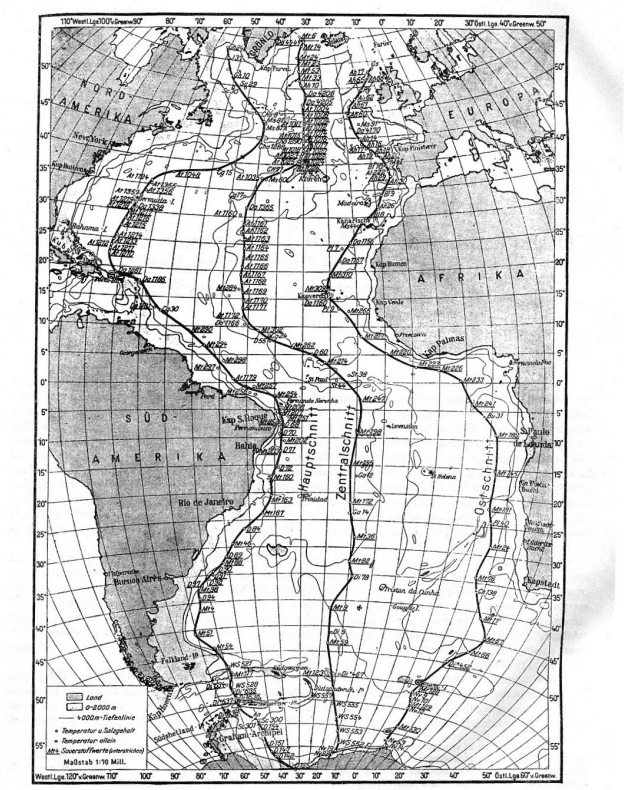

Fig. 46. Position of the stations in the three longitudinal sections.

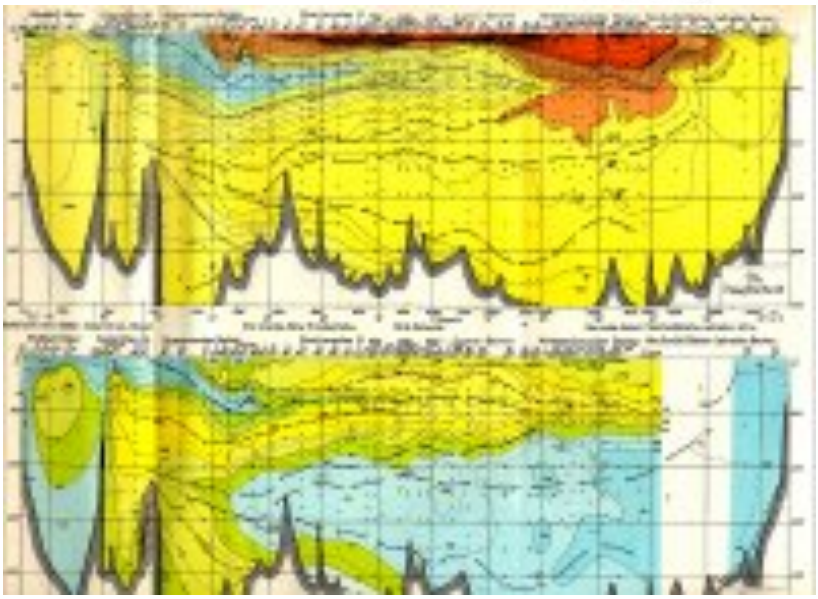

Figure 5.13: 1927-1929 Meteor Expedition, the first accurate hydrographic survey of the Atlantic from Wüst [1935]. Lower panel: Salinity and dissolved oxygen on the Hauptschnitt along the western side of the Atlantic.

Exercise 43 – Ocean thermohaline circulation

Consider a geostrophic flow (u, v)

$$-fv = -\frac{1}{\rho_0}\frac{\partial p}{\partial x} \tag{5.78}$$

$$fu = -\frac{1}{\rho_0}\frac{\partial p}{\partial y} \quad . \tag{5.79}$$

Use the hydrostatic approximation

$$\frac{\partial p}{\partial z} = -g\rho \tag{5.80}$$

and equation (5.78) in order to derive the meridional overturning stream function $\Phi(y, z)$ as a fuction of density ρ at the basin boundaries! Φ is defined via

$$\Phi(y, z) = \int_0^z \frac{\partial \Phi}{\partial \tilde{z}}\, d\tilde{z} \tag{5.81}$$

$$\frac{\partial \Phi}{\partial \tilde{z}} = \int_{x_e}^{x_w} v(x, y, \tilde{z})\, dx \quad \text{(zonally integrated transport)}, \tag{5.82}$$

where x_e and x_w are the eastward and westward boundaries in the ocean basin (think e.g. of the Atlantic Ocean). Units of Φ are $m^3 s^{-1}$. At the surface $\Phi(y, 0) = 0$.

Solution of Exercise 43: Ocean thermohaline circulation

$$\frac{\partial \Phi}{\partial z} = \int_{x_e}^{x_w} v(x, y, z)\, dx \tag{5.83}$$

$$= \frac{1}{\rho_0 f}\int_{x_e}^{x_w} \frac{\partial p}{\partial x}\, dx = \frac{1}{\rho_0 f}(p(x_w, y, z) - p(x_e, y, z)) \tag{5.84}$$

$$= -\frac{g}{\rho_0 f}\int_0^z (\rho(x_w, y, z') - \rho(x_e, y, z'))dz' \tag{5.85}$$

Exercise 44 – Estimates of overturning

It is observed that water sinks in to the deep ocean in polar regions of the Atlantic basin at a rate of 15 Sv. (Atlantic basin: $80,000,000\,km^2 area \times 4\,km$ depth.)

1. How long would it take to 'fill up' the Atlantic basin?
2. Supposing that the local sinking is balanced by large-scale upwelling, estimate the strength of this upwelling. Hint: Upwelling $= area \times w$. Express your answer in $m\ y^{-1}$.
3. Compare this number with that of the Ekman pumping in (5.31)!

Solution of Exercise 44: Estimates of overturning

1. Timescale T to 'fill up' the Atlantic basin:

$$T = \frac{80 \cdot 10^{12}\, m^2 \cdot 4000\, m}{15 \cdot 10^6\, m^3 s^{-1}} = 2.13 \cdot 10^{10} s = 676\ years$$

2. Overturning is balanced by large-scale upwelling:

$$area \cdot w = 15 \cdot 10^6\, m^3 s^{-1}$$

$$w = 0.1875 \cdot 10^{-6} m\ s^{-1} = 5.9 \cdot 10^{-15} m\ y^{-1}.$$

3. Ekman pumping

$$w_E \simeq 32\ m\ y^{-1}.$$

Simple model of meridional overturning

It is instructive to derive a simple concept of the meridional overturning based on vorticity dynamics in the (y,z)-plane. The dynamical model in two dimensions reads

$$\frac{\partial}{\partial t}v = -\frac{1}{\rho_0}\frac{\partial p}{\partial y} - fu - \kappa v \tag{5.86}$$

$$\frac{\partial}{\partial t}w = -\frac{1}{\rho_0}\frac{\partial p}{\partial z} - \frac{g}{\rho_0}(\rho - \rho_0) - \kappa w \tag{5.87}$$

with κ as parameter for Rayleigh friction. Using the continuity equation

$$0 = \frac{\partial v}{\partial y} + \frac{\partial w}{\partial z} \tag{5.88}$$

one can introduce a streamfunction $\Phi(y,z)$ with $v = \partial_z\Phi$ and $w = -\partial_y\Phi$. The associated vorticity equation in the (y,z)-plane is therefore

$$\frac{\partial}{\partial t}\nabla^2\Phi = -f\frac{\partial u}{\partial z} + \frac{g}{\rho_0}\frac{\partial \rho}{\partial y} - \kappa\nabla^2\Phi \tag{5.89}$$

We can choose the ansatz[6] satisfying that the normal velocity at the boundary vanishes, $\Phi = 0$:

$$\Phi(y,z,t) = \Phi_{max}(t)\ \sin\left(\frac{\pi y}{L}\right) \times \sin\left(\frac{\pi z}{H}\right) \tag{5.91}$$

The parameters L and H dentote the meridional and depth extend (y goes from 0 to L, z from 0 to H). With the assumption that the term $-f\frac{\partial u}{\partial z}$ is absorbed into the viscous terms, and the integration

[6] In principle, a complete Galerkin approximation shall be applied

$$\Phi(y,z,t) = \Sigma_{k=1}^{\infty}\Sigma_{l=1}^{\infty}\Phi_{max}^{k,l}(t)\ \sin(\pi k y/L) \times \sin(\pi l z/H) \tag{5.90}$$

yielding a first order differential equation in time for $\Phi_{max}^{k,l}(t)$. For a different approach: [Maas, 1994], for an overview of simple climate models: [Olbers, 2001].

$\int_0^L dy \int_0^H dz$, we derive for the three remaining terms in (5.89):

$$\frac{d}{dt}\Phi_{max}\left(\frac{\pi^2}{L^2}+\frac{\pi^2}{H^2}\right)\int_0^L dy \sin\left(\frac{\pi y}{L}\right)\int_0^H dz \sin\left(\frac{\pi z}{H}\right) = 4LH\left(\frac{1}{L^2}+\frac{1}{H^2}\right)\frac{d}{dt}\Phi_{max}$$

$$\int_0^L dy \int_0^H dz \frac{g}{\rho_0}\frac{\partial \rho}{\partial y} = \frac{g}{\rho_0} \quad H \quad (\rho_{north}-\rho_{south})$$

$$\kappa\Phi_{max}\left(\frac{\pi^2}{L^2}+\frac{\pi^2}{H^2}\right)\int_0^L dy \sin\left(\frac{\pi y}{L}\right)\int_0^H dz \sin\left(\frac{\pi z}{H}\right) = \kappa \quad 4LH\left(\frac{1}{L^2}+\frac{1}{H^2}\right)\Phi_{max}$$

with $\rho_{north} = \rho(y = L)$, and $\rho_{south} = \rho(y = 0)$, and the equation

$$\frac{d}{dt}\Phi_{max} = \frac{a}{\rho_0}(\rho_{north}-\rho_{south}) - \kappa\Phi_{max} \tag{5.92}$$

with $a = gLH^2/4(L^2+H^2)$.

This shows that the overturning circulation depends on the density differences on the right and left boxes. In the literature, (5.92) is simplified to a diagnostic relation

$$\Phi_{max} = \frac{a}{\rho_0\,\kappa}\,(\rho_{north}-\rho_{south}) \tag{5.93}$$

because the adjustment of Φ_{max} is quasi-instantaneous due to adjustment processes, e.g. Kelvin waves.

Here, we introduce a hemispheric (Stommel-type) or interhemispheric (Rooth-type) box model of the thermohaline circulation. The common assumption of these box models is that the oceanic overturning rate Φ can be expressed by the meridional density difference:

$$\Phi = -c\,(\alpha\Delta T - \beta\Delta S) \quad , \tag{5.94}$$

where α and β are the thermal and haline expansion coefficients, $c = a(\rho_0\kappa)^{-1}$, and Δ denotes the meridional difference operator applied to temperature T and salinity S, respectively. The

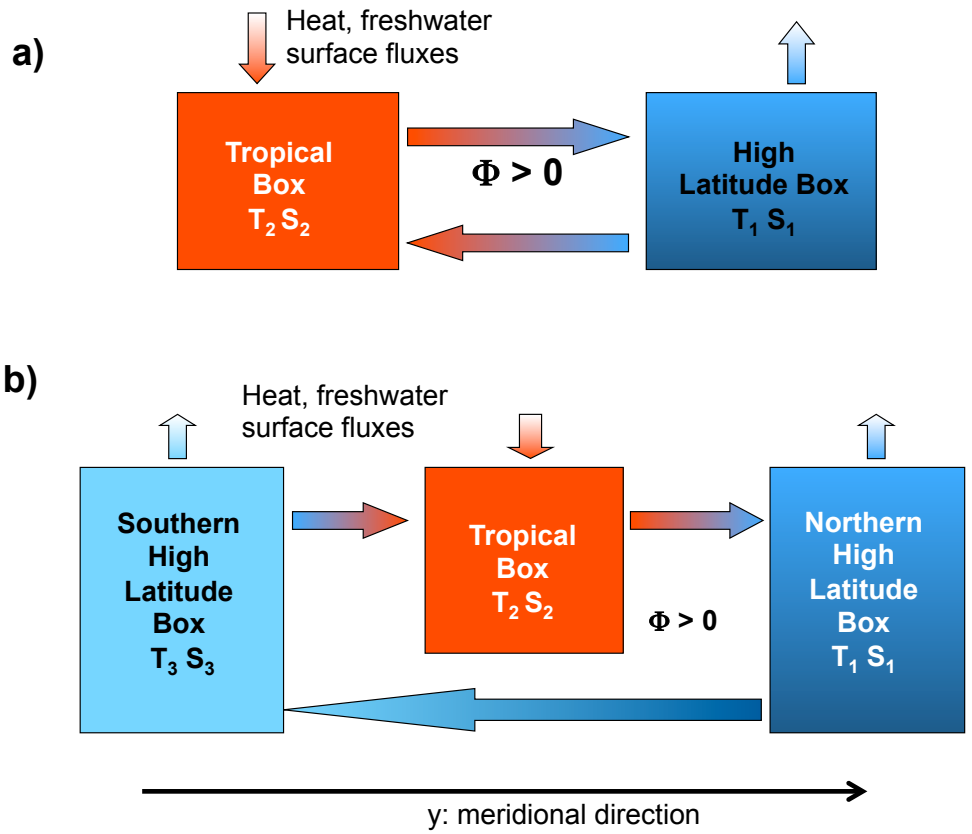

Figure 5.14: Schematic picture of the hemispheric two box model (a) and of the interhemispheric box model (b).

meriodional density differences are clearly dominated by temperature differences (Fig. 5.15a). In a single hemispheric view, the salinity difference breakes the temperature difference.

In the model of (Rooth, 1982) the Atlantic ocean is described over both hemispheres and the densities have to be taken in the North Atlantic and South Atlantic Ocean, respectively. In the interhemispheric model the densities at high northern and southern latitudes are close, the pole-to-pole differences are caused by salinity differences (Fig. 5.15b).

5.2.1 Conceptual model of the ocean circulation: Stommel's box model

The foundational paper on the analysis of the ocean circulation is by Stommel [1961] who proposes and analyzes simple "box models". This paper culminates in the analysis of the equilibrium

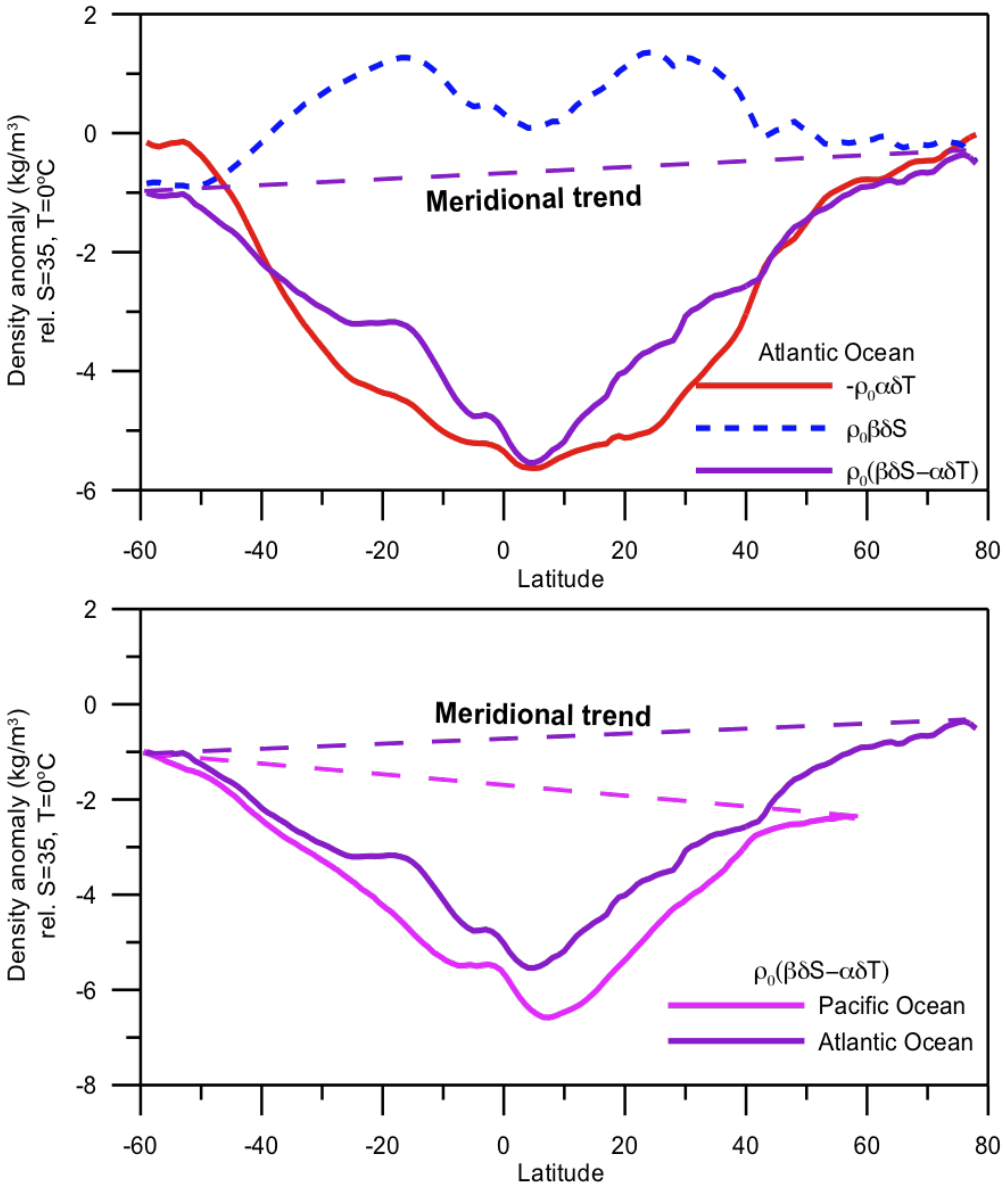

Figure 5.15: a) The Atlantic surface density is mainly related to temperature differences. b) But the pole-to-pole differences are caused by salinity differences.

solutions of a system in which two vessels connected to reservoirs are joined by a capillary that exchanges heat and salt (Fig. 5.16).

One reservoir is warm and salty, the other cold and fresh. The flow through the capillary is proportional to the difference in density of the two water masses, which is taken to be a linear

function of temperature and salinity. Upon substituting the equation of state into the equations governing the evolution of the water masses, Stommel finds two coupled nonlinear equations. In some parameter regimes there are three steady state solutions, two of which are stable. These two stable modes have opposite directions of flow, which he interprets as a competition between temperature and salinity effects on density.

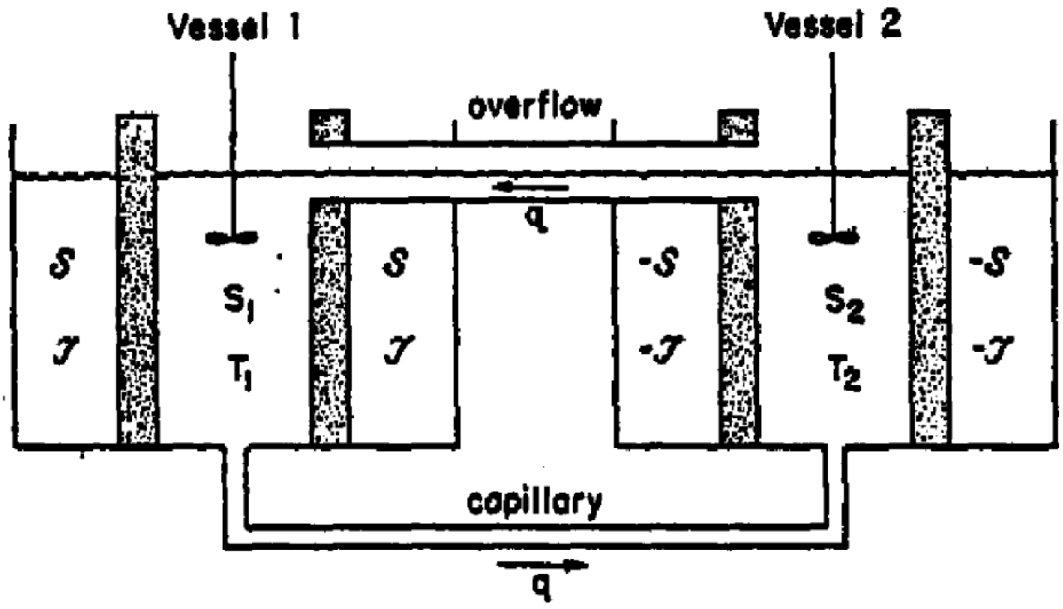

Figure 5.16: Schematic picture of the box model described by Stommel [1961].

As stated above Stommel Stommel [1961] considered a two-box ocean model where the boxes are connected by an overflow at the top and a capillary tube at the bottom (Fig. 5.16), such that the capillary flow is directed from the high density vessel to the low density vessel following with a rate Φ. The common assumption of these box models is that the oceanic overturning rate Φ can be expressed by the meridional density difference:

$$\Phi = -c\left(\alpha \Delta T - \beta \Delta S\right) \quad , \tag{5.95}$$

where α and β are the thermal and haline expansion coefficients, c is a tunable parameter, and Δ denotes the meridional difference operator applied to the variables temperature T and salinity S,

respectively. $\Delta T = T_1 - T_2$ with T_1, T_2 are the high-latitude and the tropical boxes in Fig. 5.16. The equations for temperature T and salinity S are the heat and salt budgets using an upstream scheme for the advective transport and fluxes with the atmosphere:

$$\frac{d}{dt}T_1 = \frac{\Phi}{V}T_2 - \frac{F_1^{oa}}{\rho_0 c_p h} \tag{5.96}$$

$$\frac{d}{dt}S_1 = \frac{\Phi}{V}S_2 - \frac{S_0}{h}(P-E)_1 \quad , \tag{5.97}$$

$$\frac{d}{dt}T_2 = \frac{\Phi}{V}T_1 - \frac{F_2^{oa}}{\rho_0 c_p h} \tag{5.98}$$

$$\frac{d}{dt}S_2 = \frac{\Phi}{V}S_1 - \frac{S_0}{h}(P-E)_2 \quad , \tag{5.99}$$

where V is the volume of the box with depth h, and $(P-E)$ denotes the freshwater flux (precipitation minus evaporation plus runoff). Foa is the heat flux at the ocean-atmosphere interface, S_0 is a reference salinity, and $\rho_0 c_p$ denotes the heat capacity of the ocean. Subtraction leads to

$$\frac{d}{dt}\Delta T = -\frac{\Phi}{V}\Delta T - \Delta\frac{F^{oa}}{\rho_0 c_p h} \tag{5.100}$$

$$\frac{d}{dt}\Delta S = -\frac{\Phi}{V}\Delta S - \frac{S_0}{h}\Delta(P-E) \quad . \tag{5.101}$$

The heat flux F^{oa} at the ocean-atmosphere interface can be replaced by a restoring term to the respective atmospheric temperatures, and to a first order approximation the temperatures are fixed. We now make an approximation of (5.100, 5.101) and assume that $\Delta T, c,$ and$\Delta(P-E)$ are fixed parameters. The dynamics is then given by

$$\frac{d}{dt}\Delta S = \frac{c}{V}\left(\alpha\Delta T - \beta\Delta S\right)\Delta S - \frac{S_0}{h}\Delta(P-E) \quad . \tag{5.102}$$

The steady state solution of (5.102) for ΔS can be obtained as

$$0 = \frac{c}{V}\left(\alpha\Delta T - \beta\Delta S_{eq}\right)\Delta S_{eq} - \frac{S_0}{h}\Delta(P-E) \quad , \tag{5.103}$$

which leads to a quadratic equation for

$$\Delta S_{eq} = \frac{\alpha\,\Delta T}{\beta}\left(\frac{1}{2} \pm \sqrt{\frac{1}{4} - \frac{\beta S_0 V \Delta(P-E)}{ch(\alpha\Delta T)^2}}\right) \quad . \tag{5.104}$$

It can be shown (exercise 45) that the negative root leads to an unstable solution. Furthermore

$$ch(\alpha\Delta T)^2 > 4\,\beta S_0 V \Delta(P-E) \tag{5.105}$$

which means there exists a critical $\Delta(P-E)_{crit}$ above which the flow has no solution:

$$\Delta(P-E)_{crit} = ch\frac{(\alpha\Delta T)^2}{4\,\beta S_0 V} \quad . \tag{5.106}$$

What will hapen if $\Delta(P-E) > \Delta(P-E)_{crit}$?

Stommel [1961] modified equation (5.95) to

$$\Phi \;=\; -c\,|\alpha\Delta T - \beta\Delta S| \tag{5.107}$$

Then the steady-state solutions are classified according to the sign of $q = \alpha\Delta T - \beta\Delta S$. When $q > 0$, the circulation is driven by the thermal contrast. When $q < 0$, the haline contrast is dominant in driving the current.

Exercise 45 – Bifurcation of Stommel's model

Consider Fig. 5.16 where the ocean surface water is heated at the equatorial region and flows toward high latitudes. At the pole the water is cooled and sinks, upwelling is at the equator.

1. Starting from (5.102), calculate the linear stability of the equilibrium solution (5.104).
2. Investigate the sensitivity of the stability with respect to $(P-E)_{crit}$ and the other parameters in the model.

Solution for Bifurcation of Stommel's model

We rewrite (5.102) into

$$\frac{V}{c}\frac{d}{dt}\beta\Delta S = (\alpha\Delta T - \beta\Delta S)\,\beta\Delta S - \frac{\beta S_0 V}{ch}\Delta(P-E) \quad . \tag{5.108}$$

Denoting $x=\beta\Delta S, \quad a=\alpha\Delta T, \quad b=\frac{\beta S_0 V}{ch}\Delta(P-E),$ and a non-dimentional time $t_d = t\frac{c}{V}$, we have

$$\frac{d}{dt_d}x = (a-x)\cdot x - b \tag{5.109}$$

The equilibrium solutions are

$$x_{1,2} = \frac{a}{2} \pm \sqrt{\frac{a^2}{4} - b} \tag{5.110}$$

Therefore, (5.109) can be rewritten as

$$\frac{d}{dt_d}x = f(x) = -(x-x_1)\cdot(x-x_2) \tag{5.111}$$

The derivative is

$$f'(x) = -(x-x_1) - (x-x_2) \tag{5.112}$$

and

$$f'(x_1) = -(x_1 - x_2) = -2\sqrt{\frac{a^2}{4} - b} < 0 \qquad \textbf{stable} \tag{5.113}$$

$$f'(x_2) = -(x_2 - x_1) = +2\sqrt{\frac{a^2}{4} - b} > 0 \qquad \textbf{unstable} \tag{5.114}$$

Furthermore,

$$b < \frac{a^2}{4} \quad \text{which means that} \tag{5.115}$$

$$\Delta(P-E) < \Delta(P-E)_{crit} = ch\frac{(\alpha\Delta T)^2}{4\,\beta S_0 V} \quad . \tag{5.116}$$

Reversed mode of the model: What happens if $\Delta(P-E) > \Delta(P-E)_{crit}$?

Then the direction of the circulation is anti-clockwise and the current is driven predominantly by haline contrast with higher density at low latitudes. The equation has to modified according to (5.107) and the equilibrium solutions are

$$x_{3,4} = \frac{a}{2} \pm \sqrt{\frac{a^2}{4} + b} \tag{5.117}$$

This solution has the requirement that $\frac{a^2}{4} + b > 0$. Let us now look on the linear stability of $x_{3,4}$

$$\frac{d}{dt_d}x = f(x) = (x - x_3) \cdot (x - x_4) \tag{5.118}$$

The derivative is

$$f'(x) = (x - x_3) + (x - x_4) \tag{5.119}$$

and

$$f'(x_3) = (x_3 - x_4) = +2\sqrt{\frac{a^2}{4} + b} > 0 \qquad \textbf{unstable} \tag{5.120}$$

$$f'(x_4) = (x_4 - x_3) = -2\sqrt{\frac{a^2}{4} + b} < 0 \qquad \textbf{stable} \tag{5.121}$$

This means tha tthere exists two stable equilibria (Fig. 5.17) for

$$-\frac{a^2}{4} < b = 2\frac{\beta S_0 V}{ch}(P - E) < \frac{a^2}{4} = \frac{(\alpha \Delta T)^2}{4} \quad . \tag{5.122}$$

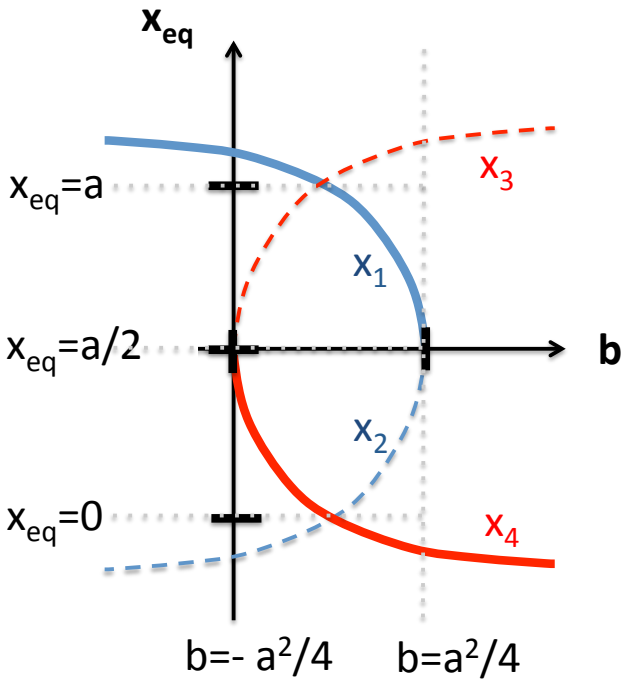

Figure 5.17: Schematic bifurcation of the Stommel box model. Dashed solutions are unstable, the solid red and blue lines represent the stable solutions, x_1 and x_4, respectively.

5.2.2 Non-normal dynamics of the ocean box model*

In this section, a category of the non-linear models following the simple thermohaline model of Stommel Stommel [1961] is analyzed. We start with (5.100, 5.101). Denoting furthermore $\boldsymbol{x} \in \mathbf{R}^2$ for the anomalies of $(\boldsymbol{\Delta T}, \boldsymbol{\Delta S})$, Lohmann and Schneider **?** have shown that the evolution equation is of the following structure:

$$\frac{\boldsymbol{d}}{\boldsymbol{dt}}\boldsymbol{x} \;=\; \boldsymbol{A}\boldsymbol{x} \;+\; \langle\, \boldsymbol{b} | \boldsymbol{x} \,\rangle \;\; \boldsymbol{x}\,. \tag{5.123}$$

The brackets $\langle \mid \rangle$ denote the Euclidean scalar product. This evolution equation (5.123) can be transferred to a

$$\boldsymbol{x}(\boldsymbol{t}) \;=\; \frac{\mathbf{1}}{\boldsymbol{\gamma}(\boldsymbol{t})} \;\; \mathbf{exp}(\boldsymbol{A}\boldsymbol{t})\, \boldsymbol{x_0}\;, \tag{5.124}$$

with a scaling function $\boldsymbol{\gamma}(\boldsymbol{t}, \boldsymbol{x_0})$. The models of Stommel **?**, and many others are of this type, and their dynamics are therefore exactly known. [7]

It is useful to analyze the dynamics in the phase space spanned by temperature and salinity anomalies and investigate the model sensitivity under anomalous high latitude forcing, induced as an initial perturbation. The lines in Fig. 5.18 are phase space trajectories after perturbations of different magnitude have been injected into the North Atlantic. We notice that for most trajectories, the distances from zero $(\mathbf{0}, \mathbf{0})$ increase temporarily, where the maximal distance from zero is after a decade. After about $\mathbf{10}$ years the trajectories in Fig. 5.18 point into a "mixed temperature/salinity direction", denoted further as $\boldsymbol{e_1}$.

Fig. 5.18 implies that the adjustment of the THC involves two phases: A fast thermal response and a slower response on the $\boldsymbol{e_1}-$direction. The vector $\boldsymbol{e_1}$ is identical with the most unstable mode in the system. Because the scaling function $\boldsymbol{\gamma}(\boldsymbol{t})$ acts upon both temperature and salinity (5.124), the evolution of the non-linear model can be well characterized by the eigenvectors of the matrix

[7] It is worth knowing that (5.100, 5.101) is equivalent to the multi-dimensional Malthus-Verhulst model (also known as logistic equation), which was originally proposed to describe the evolution of a biological population.

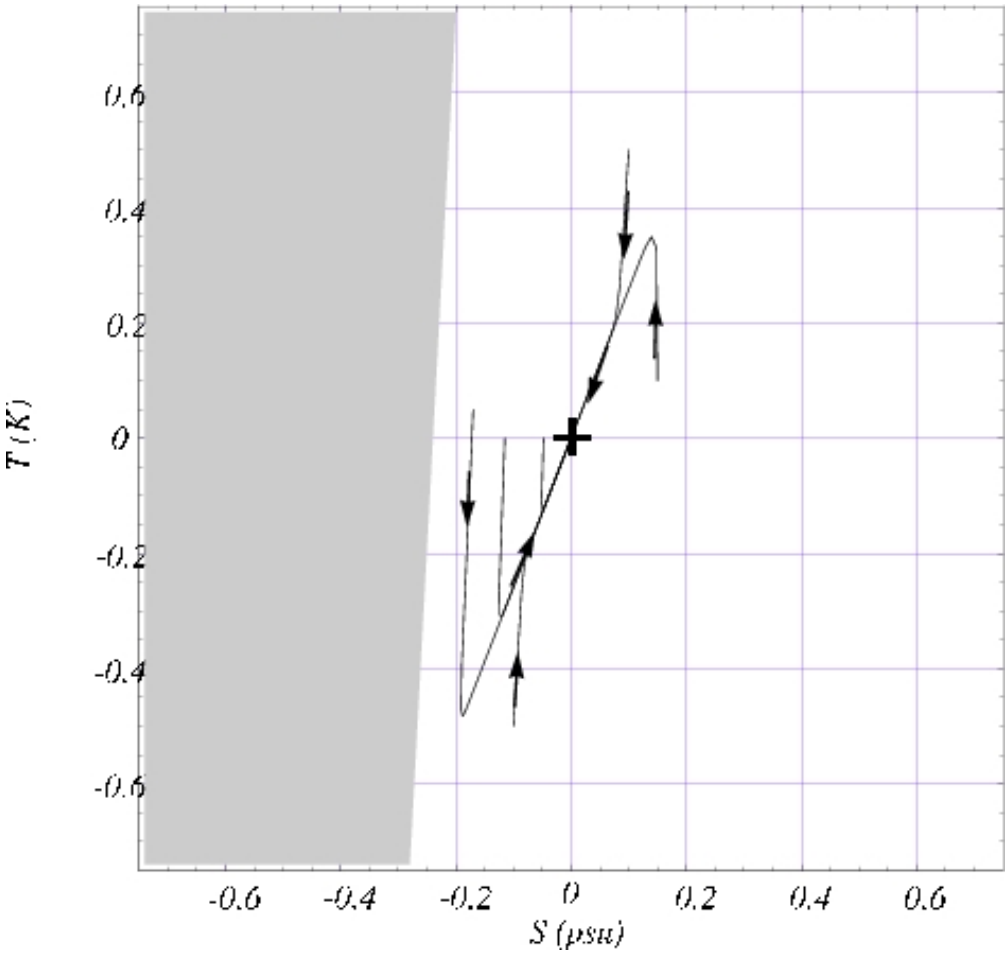

Figure 5.18: The basin of attraction (white area) and the dynamics in the thermohaline phase space. With initial conditions outside the gray area, the trajectories converge asymptotically to the origin corresponding to the thermally driven solution of the THC. Due to the fast thermal response during the first decade of relaxation, the distance of the trajectories from zero can increase temporarily.

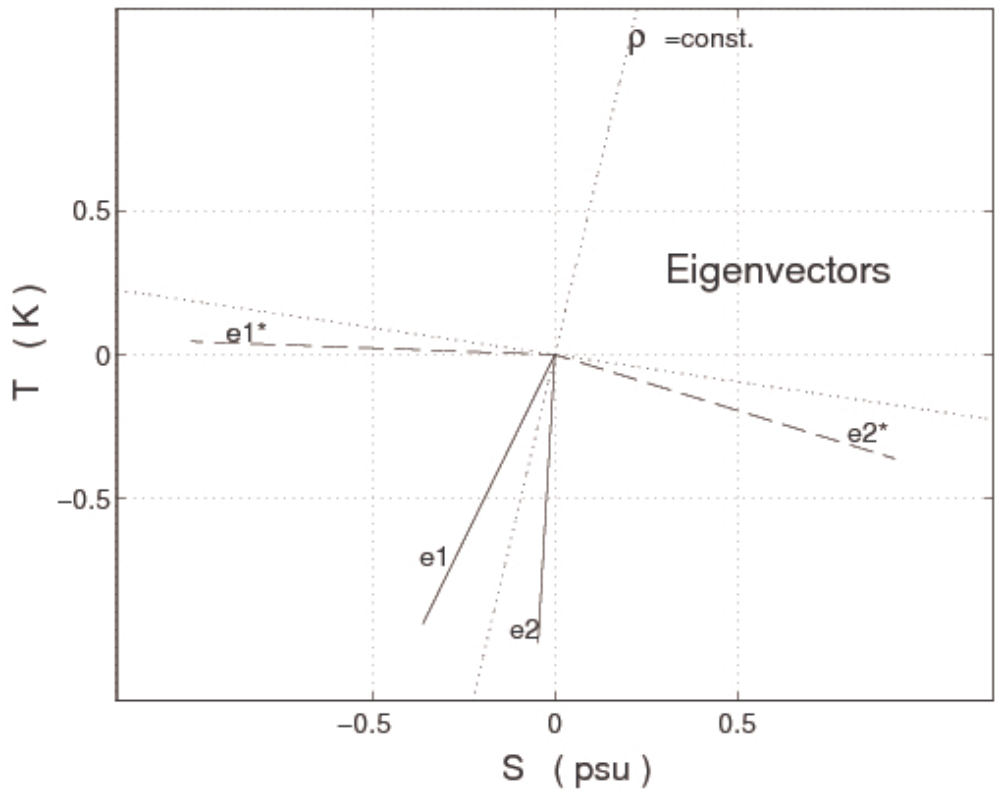

Figure 5.19: Eigenvectors e_1, e_2, and adjoint eigenvectors e_1^*, e_2^* of the tangent linear operator A^+ . The dotted lines show the line of constant density and the perpendicular.

$\boldsymbol{A}$, which is discussed in the following.

In our system, the operator $\boldsymbol{A}$ of the box model is found to be non-normal, and the eigenvectors are not orthogonal. One eigenvalue $(\boldsymbol{e_2})$ is closely related to temperature anomalies, whereas the other $(\boldsymbol{e_1})$ is a "mixed temperature/salinity eigenvector" (Fig. 5.19). The eigenvectors of the adjoint matrix $\boldsymbol{A^+}$ are denoted by $\boldsymbol{e_1^*}$ and $\boldsymbol{e_2^*}$, respectively. For the non-normal matrix $\boldsymbol{A}$, the eigenvectors of $\boldsymbol{A}$ and $\boldsymbol{A^+}$ do not coincide, but fulfill the "biorthogonality condition":

$$\boldsymbol{e_1^* \perp e_2} \text{ and } \boldsymbol{e_2^* \perp e_1}\,. \tag{5.125}$$

Both eigenvalues $\boldsymbol{\lambda_{1,2}}$ are real and negative. Because of $\boldsymbol{\lambda_2 < \lambda_1}$, the first term dominates for long time scales and the second for short time scales. Using the biorthogonality condition, we get furthermore the coefficients

$$\boldsymbol{c_i = \frac{\langle e_i^* | x_0 \rangle}{\langle e_i^* | e_i \rangle}} \qquad \text{for} \qquad \boldsymbol{i = 1, 2} \tag{5.126}$$

A perturbation is called "optimal", if the initial error vector has minimal projection onto the subspace with the fastest decaying perturbations, or equivalently if the coefficient $\boldsymbol{c_1}$ is maximal. This is according to (5.126) equivalent to $\boldsymbol{x_0}$ pointing into the direction of $\boldsymbol{e_1^*}$. This unit vector $\boldsymbol{e_1^*}$ is called the "biorthogonal" **?** to the most unstable eigenvector $\boldsymbol{e_1}$ which we want to excite. In order to make a geometrical picture for the mathematical considerations, assume that the tail of the vector $\boldsymbol{x_0}$ is placed on the $\boldsymbol{e_1}-$line and its tip on the $\boldsymbol{e_2}-$line. This vector is stretched maximally because the tail decays to zero quickly, whereas the tip is hardly unchanged due to the larger eigenvalue $\boldsymbol{\lambda_1}$. The most unstable mode $\boldsymbol{e_1}$ and its biorthogonal $\boldsymbol{e_1^*}$ differ greatly from each other, and the perturbation that optimally excites the mode bears little resemblance to the mode itself.

It is remarkable that the optimal initial perturbation vector $\boldsymbol{e_1^*}$ does not coincide with a perturbation in sea surface density at high latitudes, which would reside on the dotted line perpendicular to $\boldsymbol{\rho = const.}$ in Fig. 5.19. Even when using a space spanned by $\boldsymbol{(\alpha T, \beta S)}$ instead of $\boldsymbol{(T, S)}$,

to take into account the different values for the thermal and haline expansion coefficients, vector e_1^* is much more dominated by the scaled salinity anomalies than the temperature anomalies of the high latitudinal box.

Numerical simulations by Manabe and Stouffer Manabe and Stouffer [1993] showed, for the North Atlantic, that between two and four times the preindustrial CO_2 concentration, a threshold value is passed and the thermohaline circulation ceases completely. One other example of early Holocene rapid climate change is the '8200 yr BP' cooling event recorded in the North Atlantic region possibly induced by freshwater. One possible explanation for this dramatic regional cooling is a shutdown in the formation of deep water in the northern North Atlantic due to freshwater input caused by catastrophic drainage of Laurentide lakes Barber et al. [1999]; Lohmann [2003]. The theoretic considerations and these numerical experiments suggest that the formation of deep water in the North Atlantic is highly sensitive to the freshwater forcing.

Part III

Third part: Stochastic climate model and Mesoscopic Dynamics

Part IV

Fourth part: Programming and tools

Bibliography

Abramowitz, M. and Stegun, I. A. (1965). Handbook of mathematical functions with formulas, graph, and mathematical tables. *Applied Mathematics Series*, 55:1046.

Arnold, L. (1995). *Random dynamical systems*. Springer.

Arnold, L. (2001). *Hasselmann's program revisited: The analysis of stochasticity in deterministic climate models*, volume 49. Birkhäuser, Boston.

Baker, G. L. and Blackburn, J. A. (2005). *The pendulum: a case study in physics*, volume 8. Oxford University Press Oxford.

Barber, D., Dyke, A., Hillaire-Marcel, C., Jennings, J., Andrews, J., Kerwin, M., Bilodeau, G., McNeely, R., Southon, J., Morehead, M., and Gagnonk, J.-M. (1999). Forcing of the cold event of 8,200 years ago by catastrophic drainage of laurentide lakes. *Nature*, 400(6742):344–348.

Bhatnagar, P., Gross, E. P., and Krook, M. K. (1954). A model for collision process in gases. i. small amplitude processes in charged and neutral one-component system. *Phys. Rev*, 94:511.

Boltzmann, L. (1896). *Vorlesungen über Gastheorie : 2 Volumes (in German)*. Leipzig 1895/98 UB: O 5262-6.

Boltzmann, L. (1995). *Lectures on Gas Theory*. Dover Publ. New York. ISBN 978-0486684550.

Broecker, S. and Peng, T.-H. (1982). *Tracers in the Sea*. Columbia University.

Broecker, W. S. (1987). The biggest chill. *Natural History*, 97(2):74–82.

Broecker, W. S. et al. (1991). The great ocean conveyor. *Oceanography*, 4(2):79–89.

Brüning, R. and Lohmann, G. (1999). Charles s. peirce on creative metaphor: a case study on the conveyor belt metaphor in oceanography. *Foundations of science*, 4(4):389–403.

Bryan, F. (1986). High latitude salinity effects and inter-hemispheric thermohaline circulations. *Nature*, 323(3):301–304.

Buckingham, E. (1914). On physically similar systems; illustrations of the use of dimensional equations. *Physical Review*, 4(4):345–376.

Budyko, M. I. (1969). The effect of solar radiation variations on the climate of earth. *Tellus*, 21:611–619.

Busch, W. (1865). *Max und Moritz (in German); Max and Maurice, a Juvenile History in Seven Tricks* . Braun und Schneider, München.

Cercignani, C. (1987). *The Boltzmann equation and its applications*. Springer New York. ISBN 978-0387966373.

Cercignani, C. (1990). *Mathematical methods in kinetic theory*. Plenum, 2 edition. ISBN 978-0306434600.

Chelton, D. B. and Schlax, M. G. (1996). Global Observations of Oceanic Rossby Waves. *Science*, 272:234–238.

Chen, D., Gerdes, R., and Lohmann, G. (1995). A 1-d atmospheric energy balance model developed for ocean modelling. *Theoretical and Applied Climatology*, 51:25–38.

Chorin, A. J. and Hald, O. H. (2006). Stochastic tools in mathematics and science. surveys and tutorials in the applied mathematical sciences, vol. 1.

Chorin, A. J., Kast, A. P., and Kupferman, R. (1999). Unresolved computation and optimal predictions. *Communications on pure and applied mathematics*, 52(10):1231–1254.

Chorin, A. J., Kupferman, R., and Levy, D. (2000). Optimal prediction for hamiltonian partial differential equations. *Journal of Computational Physics*, 162(1):267–297.

Courant, R., Friedrichs, K., and Lewy, H. (1928). Über die partiellen Differenzengleichungen der mathematischen Physik. *Mathematische Annalen*, 100:32–74.

Courant, R., Friedrichs, K., and Lewy, H. (1967). On the partial difference equations of mathematical physics. *IBM J. Res. Dev.*, 11(2):215–234.

Dansgaard, W., Johnsen, S., Clausen, H., Dahl-Jensen, D., Gundestrup, N., Hammer, C., C.S. Hvidberg, J. S., Sveinbjoernsdottir, A., Jouzel, J., and Bond, G. (1993). Evidence for general instability of past climate from a 250-kyr ice-core record. *Nature*, 364:218–220.

d'Humieres, D., Bouzidi, M., and Lallemand, P. (2001). Thirteen-velocity three-dimensional lattice boltzmann model. *PRE*, 63(6, Part 2).

Dijkstra, H., Raa, L. T., and Weijer, W. (2004). A systematic approach to determine thresholds of the ocean's thermohaline circulation. *Tellus A*, 56 (4):362.

Doedel, E. J., Champneys, A. R., Fairgrieve, T. F., Kuznetsov, Y. A., Sandstede, B., and Wang, X. (1997). Continuation and bifurcation software for ordinary differential equations (with homcont). *Available by anonymous ftp from ftp cs concordia ca, directory pub/doedel/auto*.

Egger, J. (2001). Master equations for climatic parameter sets. *Climate Dynamics*, 18(1-2):169–177.

Einstein, A. (1905). Investigations on the theory of the brownian movement. *Ann. der Physik*, 17:549–560.

Einstein, A. (1926). Die Ursache der Mäanderbildung der Flußläufe und des sogenannten Baerschen Gesetzes. *Naturwissenschaften*, 14:223–224.

Evans, D. J. and Morriss, G. (2008). *Statistical mechanics of nonequilibrium liquids*. Cambridge University Press.

Fairbanks, R. G. (1989). A 17, 000-year glacio-eustatic sea level record: influence of glacial melting rates on the younger dryas event and deep-ocean circulation. *Nature*, 342(6250):637–642.

Feigenbaum, M. J. (1980). The transition to aperiodic behaviour in turbulent systems. *Commun. Math. Phys.*, 77.

Flammer, C. (1957). *Spheroidal wave functions*. Stanford University Press.

Frisch, U. (1996). *Turbulence: the legacy of A.N. Kolmogorov*. Cambridge University Press. ISBN 0-521-45103-5.

Gerkema, T., Zimmerman, J., Maas, L., and Van Haren, H. (2008). Geophysical and astrophysical fluid dynamics beyond the traditional approximation. *Reviews of Geophysics*, 46(2).

Gill, A. E. (1982). *Atmosphere-ocean dynamics*, volume 30. Academic Press. International Geophysics Series.

Givon, D., Kupferman, R., and Stuart, A. (2004). Extracting macroscopic dynamics: model problems and algorithms. *Nonlinearity*, 17(6):R55.

Gottwald, G. (2010). On recent trends in climate dynamics. *AMS Gazette*, 37(5).

Grassberger, P. and Procaccia, I. (1983). Measuring the strangeness of strange attractors. *Physica D: Nonlinear Phenomena*, 9(2):189–208.

Haken, H. (1996). Slaving principle revisited. *Physica D: Nonlinear Phenomena*, 97(1):95–103.

Haney, R. L. (1971). Surface thermal boundary conditions for ocean circulation models. *Journal of Physical Oceanography*, 1:241–248.

Hasselmann, K. (1976). Stochastic climate models. Part I. Theory. *Tellus*, 6:473–485.

He, X. and Luo, L. S. (1997). Theory of the lattice Boltzmann method: From the Boltzmann equation to the lattice Boltzmann equation. *Phys. Rev. E*, 56(6):6811–6817.

Holton, J. R. (2004). *An Introduction to Dynamic Meteorology*. Elsevier Academic Press, Burlington, MA.

Kambe, T. (2007). *Elementary Fluid Mechanics*. World Scientific Publishing.

Kuznetsov, Y. A. (1998). *Elements of applied bifurcation theory*, volume 112. Springer, New York.

Landau, L. D. and Lifshitz, E. M. (1959). *Fluid Mechanics*, volume 6 of *Course of Theoretical Physics*. Pergamon Press, Oxford.

Langevin, P. (1908). On the theory of brownian motion. *Comptes Rendues*, 146:530–533.

Leith, C. (1975). Climate response and fluctuation dissipation. *Journal of the Atmospheric Sciences*, 32(10):2022–2026.

Lohmann, G. (2003). Atmospheric and oceanic freshwater transport during weak atlantic overturning circulation. *Tellus A*, 55(5):438–449.

Longuet-Higgins, M. S. (1968). The eigenfunctions of laplace's tidal equations over a sphere. *Philosophical Transactions for the Royal Society of London. Series A, Mathematical and Physical Sciences*, pages 511–607.

Lorenz, E. (1982). Atmospheric predictability experiments with a large numerical model. *Tellus A*, 34:505–513.

Lorenz, E. N. (1960). Maximum simplification of the dynamic equations. *Tellus*, 12(3):243–254.

Lorenz, E. N. (1963). Deterministic nonperiodic flow. *Journal of the atmospheric sciences*, 20(2):130–141.

Lorenz, E. N. (1976). Nondeterministic theories of climatic change. *Quaternary Research*, 6(4):495–506.

Lorenz, E. N. (1984). Irregularity: a fundamental property of the atmosphere*. *Tellus A*, 36(2):98–110.

Lucarini, V., Blender, R., Herbert, C., Pascale, S., Ragone, F., and Wouters, J. (2014). Mathematical and physical ideas for climate science. *Rev. Gephys.*

Maas, L. R. (1994). A simple model for the three-dimensional, thermally and wind-driven ocean circulation. *Tellus A*, 46(5):671–680.

Manabe, S. and Stouffer, R. (1993). Century-scale effects of increased atmospheric $\boldsymbol{CO_2}$ on the ocean atmosphere system. *Nature*, 364:215–218.

Mandelbrot, B. B. (1967). How long is the coast of britain: Statistical self-similarity and fractal dimension. *Science*, 155:636–638.

Mandelbrot, B. B. (1983). *The fractal geometry of nature*. Macmillan.

Matsuno, T. (1966). Quasi-geostrophic motions in the equatorial area. *J. Meteor. Soc. Japan*, 44(1):25–43.

Mori, H. (1965). Transport, collective motion, and brownian motion. *Progress of Theoretical Physics*, 33(3):423–455.

Mori, H., Fujisaka, H., and Shigematsu, H. (1974). A new expansion of the master equation. *Progress of Theoretical Physics*, 51(1):109–122.

Müller and Maier-Reimer (2000). Trapped rossby waves. *Phys. Rev. E*, 61:1468 – 1485.

Müller, D., Kelly, B., and O'brien, J. (1994). Spheroidal eigenfunctions of the tidal equation. *Physical review letters*, 73(11):1557.

Müller, D. and O'Brien, J. (1995). Shallow water waves on the rotating sphere. *Physical Review E*, 51(5):4418.

Olbers, D. (2001). A gallery of simple models from climate physics. *In: Stochastic Climate Models, Progress in Probability (Eds.: P. Imkeller and J. von Storch)*, 49:3–63.

Peitgen, H.-O. and Richter, P. (1986). *The Beauty of Fractals*. Heidelberg: Springer-Verlag.

Proudman, J. (1916). On the motion of solids in a liquid possessing vorticity. *Proc. R. Soc. Lond. A*, 92:408–424.

Rahmstorf, S. (1996). On the freshwater forcing and transport of the Atlantic thermohaline circulation. *Climate Dynamics*, 12:799–811.

Rayleigh, L. (1916). On convection currents in a horizontal layber of fluid, when the higher temperature is on the under side. *Phil. Mag.*, 6:529–546.

Rooth, C. (1982). Hydrology and ocean circulation. *Progress in Oceanography*, 11:131–149.

Rossby, C.-G. (1939). "relation between variations in the intensity of the zonal circulation of the atmosphere and the displacements of the semi-permanent centers of action". *Journal of Marine Research*, 2 (1):38–55.

Saltzman, B. (1962). Finite amplitude free convection as an initial value problem – i. *Journal of the Atmoshpheric Sciences*, 19:329–341.

Shannon, C. E. (1948). A Mathematical Theory of Communication. *Bell System Technical Journal*, 27 (3):379–423.

Stommel, H. (1961). Thermohaline convection with two stable regimes of flow. *Tellus*, 13:224–230.

Strogatz, S. (2000). *Non-linear Dynamics and Chaos: With applications to Physics, Biology, Chemistry and Engineering*. Perseus Books.

Taylor, G. (1917). Motion of solids in fluids when the flow is not irrotational. *Proc. R. Soc. Lond. A*, 93:92–113.

Townsend, S., Lenosky, T., Muller, D., Nichols, C., and Elser, V. (1992). Negatively curved graphitic sheet model of amorphous carbon. *Physical Review Letters*, 69(6):921–924.

Tritton, D. J. (1988). *Physical Fluid Dynamics*. Oxford University Press, Science Publication. ISBN 978-0-19-854493-7.

Uhlenbeck, G. E. and Ornstein, L. S. (1930). On the theory of the brownian motion. *Physical review*, 36(5):823.

van Kampen, N. G. (1981). *Stochastic processes in physics and chemistry*. North Holland. IISBN 978-0-444-52965-7.

Wüst, G. (1935). Schichtung und Zirkulation des Atlantischen Ozeans. Das Bodenwasser und die Stratosphäre. *Wiss. Ergebn. Dtsch. Atlant. Exped. 'Meteor' 1925-1927*, 6(1):1–288.

Zwanzig, R. (1960). Ensemble method in the theory of irreversibility. *The Journal of Chemical Physics*, 33:1338.

Zwanzig, R. (1980). Problems in nonlinear transport theory. In *Systems far from equilibrium*, pages 198–225. Springer.

Zwanzig, R. (2001). *Nonequilibrium statistical mechanics*. Oxford University Press, USA.